Title
1-1.4 Micron Spectral Atlas of Stars

Journal
The Astrophysical Journal Supplement Series, 142(1)

ISSN
0067-0049

Authors
Malkan, MA
Hicks, EK
Teplitz, HI
et al.

Publication Date
2002-09-01

DOI
10.1086/341176

Peer reviewed

1–1.4 Micron Spectral Atlas of Stars

M. A. Malkan [1], E. K. Hicks [1], H. I. Teplitz[2,3], I. M. McLean [1], H. Sugai[4], J. Guichard[5]

ABSTRACT

We present a catalog of J-band (1.08 μm to 1.35 μm) stellar spectra at low resolution (R $\sim$ 400). The targets consist of 105 stars ranging in spectral type from O9.5 to M7 and luminosity classes I through V. The relatively featureless spectra of hot stars, earlier than A4, can be used to remove the atmospheric features which dominate ground-based J-band spectroscopy. We measure equivalent widths for three absorption lines and nine blended features which we identify in the spectra. Using detailed comparison with higher resolution spectra, we demonstrate that low resolution data can be used for stellar classification, since several features depend on the effective temperature and gravity. For example The CN index (1.096 - 1.104 μm) decreases with temperature, but the strength of a blended feature at 1.28 μm (consisting of primarily Pβ) increases. The slope of a star's spectrum can also be used to estimate its effective temperature. The luminosity class of a star correlates with the ratio of the Mg I (1.1831 μm) line to a blend of several species at 1.16 μm. Using these indicators, a star can be classified to within several subclasses. Fifteen stars with particularly high and low metal abundances are included in the catalog and some spectral dependence on metal abundance is also found.

Subject headings: infrared: stars - line: identification - stars: fundamental parameters

---

[1]Department of Physics and Astronomy, University of California, Los Angeles, CA, 90095-1562

[2]NOAO Research Associate

[3]Laboratory for Astronomy and Solar Physics, Code 681, Goddard Space Flight Center, Greenbelt MD 20771 Electronic mail: hit@binary.gsfc.nasa.gov

[4]Department of Astronomy, Kyoto University, Sakyo-ku, Kyoto 606-8502 Japan

[5]Instituto Nacional de Astrofisica, Optica y Electronica, 20 Luis Enrique Erro 1, Tonantzintla, Puebla, 72840, Mexico

1. Introduction

The widespread availability of infrared array detectors, coupled with a new generation of infrared spectrometers (e.g. McLean 1994; McLean et al. 1998) have allowed for increasingly routine spectroscopy of astrophysically important stellar absorption lines. Near-infrared (NIR) spectroscopy is essential to the study of young and low mass stellar objects (e.g.McLean et al. 2000), as well as regions of the galaxy suffering large extinction (e.g. Figer, McLean and Morris 1999). NIR absorption lines are also being observed in composite stellar systems, such as star clusters and local galaxies (Mouhcine & Lancon 2001). Observations of the rest-frame NIR spectra of galaxies at appreciable redshift will soon be possible with SIRTF (Fanson et al. 1998) and NGST (Stockman 1997). There is consequently a growing need for accurate modeling of the NIR spectral range, which in turn must rely on NIR observations of all types of stars.

Several excellent atlases of stellar spectra have been published for the H (1.5–1.8 μm) and K (2.0–2.4 μm) atmospheric windows (Lancon & Rocca 1992; Wallace & Hinkle 1996). These data have shown that stellar atmosphere models do not *a priori* predict acceptable spectral energy distributions (SED's) in the near-IR, but must be refined based on observations. Published spectra in the J (1.05–1.35 μm) window are limited to a few specialized studies (e.g. Jones et al. 1996) and the recent atlas of Wallace et al. (2000). Though stellar spectral classification is easiest to do with high resolution data, as obtained in the above mentioned studies, lower resolution is necessary for observations of a substantial number of objects (e.g. survey of distant galaxies).

In this paper, we present the results of a spectroscopic survey of normal stars in the J-band. Using a low resolution grism we observed 105 stars in the northern hemisphere. The sample spans spectral types O9.5-M7 and luminosity classes I-V. Some preliminary results were presented in Hicks et al. (2000). The observations were taken over the course of several years, often as a "backup" program in non-photometric weather. As we outline below, care has been taken to determine the best correction for the atmospheric absorption. The observations are described in § 2, and § 3 discusses the data reduction techniques. One initial impetus for the inquiry was the need for good atmospheric standards for J-band spectroscopy of extragalactic targets, and we discuss the results of that investigation in § 3, as well. In § 4 we provide the atlas, line lists and discuss line identification. Section 5 presents a comparison with previous studies at higher resolution and § 6 discusses the trends observed in the data. A near-infrared stellar spectral classification scheme is discussed in § 7.

2. Observations

The UCLA 2-Channel spectrograph (McLean et al 1994; known colloquially as GEMINI for its twin detectors) has been used regularly during bright runs over the last 8 years on the Shane 3.0-m reflector at Lick Observatory. During this time we have obtained a large archive of J-band stellar spectroscopy, which are presented here as an Atlas for future applications. The Atlas has been assembled during an ongoing "backup" program during nights of non-photometric conditions. Supplemental observations for the Atlas were made at the start and the end of a night's observing in good weather. Additional J-band spectra were obtained to correct for atmospheric absorption in other programs.

The Atlas contains 105 stars (see Table 1), 99 selected from the Bright Star Catalog (1982) and 6 from the Henry Draper Catalog (1995). Table 1 includes the catalog name, the spectral class, effective temperature, and, when available, the metallicity. Fifty-eight are main sequence stars and 46 are giants or supergiants. Fifteen stars were chosen because high-resolution optical spectroscopy has shown that they have unusually high or low heavy-element abundances (Cayrel de Strobel et al. 1997).

All observations were made using the Rockwell HgCdTe 256 x 256 array detector and grism spectroscopy in the J-band. One pixel corresponds to about 11.6 Å, and the 2-pixel (1.5 arcseconds) wide slit yielded a typical spectral resolution of $R \sim 400$. Each star was observed consecutively in two positions, separated by 20–40 arcseconds along the North/South slit. The two images were used as the sky frames for each other, by direct subtraction. In many cases no telescope guiding was attempted during the short ($\leq$ 60 second) exposures. This sometimes resulted in the star drifting partly out of the slit during the second exposure. If the signal dropped by more than a factor of two, the star was recentered on the slit for a third exposure. In any case, the absolute flux levels are not of interest in this study. In general the spectral shape (i.e. relative fluxes from 1.05 to 1.35 μm) is accurately measured.

3. Data Reduction

All spectra were initially processed with IRAF[1] scripts based on the APEXTRACT package. After eliminating bad pixels, images were sky-subtracted and divided by a normalized flat field. The flat frame was the difference between exposures of the dome ceiling with and without an illuminating lamp. Next the top and bottom spectra were mapped, rectified,

[1]IRAF is distributed by NOAO, which is operated by AURA Inc., under cooperative agreement with the NSF

and extracted, using a 7″-long slit region, with local sky subtraction. The arithmetic average of the two spectra was obtained.

Near-IR spectroscopy, even at low resolution, requires careful sky subtraction and correction for atmospheric absorption. The strength of OH radical emission in the night sky varies rapidly with time, requiring contemporaneous sky measurements. Wavelength calibration is complicated by the density of night sky lines, which are often unresolved at low resolution; good calibration data from comparison lamps is thus required. The spectra were assigned a wavelength scale, usually obtained from a Chebyshev polynomial fit to 11–13 isolated arc lines in the spectra of a comparison lamp of Kr, Ar, or Ar with Ne. The GEMINI spectrograph has been shown to be stable (see Sugai et al. 1997) allowing the use of calibration data taken at the end of the night or even the following night. In a few cases the wavelength calibrations were obtained after a longer gap in time during the observing run. As a result, wavelength shifts of up to 1 or 2 pixels (11.6 Å to 23.2 Å) sometimes occurred. In the worst case, the wavelength scales of these stellar spectra were re-calibrated using the strongest OH night-sky lines visible in the stellar spectra themselves. The resulting wavelengths, using either a comparison lamp or sky lines, are accurate to better than one pixel, with $\sigma(\lambda) \sim 8$ Å, except where indicated in Table 3. Data taken during the September 1999 run have less accurate wavelength scales because the grism wheel motions were not completely repeatable, resulting in an increased uncertainty in the calibration of 15 Å. Typical examples of arcs and night-sky lines are shown in Figure 1. The measured full width at half-max (FWHM) of arc lines and night-sky lines is 2.4 to 2.8 pixels (28 to 32 Å).

The final step in the reduction is the atmospheric absorption correction. Stellar spectra were divided by a telluric extinction template spectrum (see Figure 2). Stars hotter than A4 (8550 K) have only two detectable absorption features (Pγ and Pβ), and so may be used to create atmospheric templates. After interpolating across these features what remains is purely atmospheric absorption. We used a uniform template to correct all the stellar data (with the exception of the September 1999 run, which was calibrated separately). This template spectrum consists of two parts: the average of six spectra of A1V stars in the wavelength interval 1.15–1.35 μm together with the average of one A3V and two A1V stars for the 1.07–1.10 μm region. The September 1999 run data were corrected for telluric absorption using the average of three A0 and two A2 stars taken during that run. In all of the stellar data, the worst region of atmospheric absorption, from 1.10–1.15 μm, could not be fully corrected.

Three other atmospheric absorption template spectra were used to confirm the validity of our results. The first check used the average of seven A3V stars from our own data. We also compared our results to those obtained when using the absorption templates from

Wallace et al. (1996) and Hinkle & Wallace (1995); those authors created high dispersion absorption templates in order to correct their observations of the Sun (spectral type G2V) and of Arcturus (spectral type K2III), respectively. Each of these atmospheric template spectra yield results similar to those given by the template originally used, confirming that our choice of templates removes the atmospheric absorption adequately.

The spectra in the Atlas have excellent photon statistics, with over ten thousand photons detected per pixel. The repeatability of the spectra measured at the top and bottom slit positions confirms that errors due to sky subtraction and flat fielding are also below 1%, except in the 1.10–1.15 μm atmospheric absorption trough. The typical signal to noise ratio (SNR) in each spectrum is better than 100 per 2.5-pixel (30 Å) resolution element. Thus, absorption lines down to 1 Å equivalent width (or 2 Å in the most uncertain part of the spectrum which is heavily affected by atmospheric absorption) can be measured.

The data reduction process altered the intrinsic slope of the stellar spectra, though in a predictable way. The steps in our reduction process that could alter the slope are the division by a flat field and the division by the atmospheric template. With each run, flat fields with a slightly different wavelength dependence were used. Since the wavelength dependence was not removed, this caused the spectra from different observing runs to have slopes that differ by as much as a factor of three for stars of a similar spectral type (which are expected to have similar spectral slopes). These spectra were then divided by an atmospheric absorption A star template that was created from an average of several A stars from different runs. Had the spectra been divided by a template created from only A stars observed on the same run, and thus corrected with the same flat field, then stars of the same spectral type from all runs would have similar slopes. However, to create a high quality atmospheric template it was necessary to average A stars from several different observing runs. The resulting slopes of the spectra were thus dependent on the run in which they were observed. The dependence was removed by determining the correction necessary to force A1V stars to have a slope of zero, which would be expected after dividing by an atmospheric template made from A1V stars. This correction was determined for each run separately. The resulting slope is then a differential slope that is the ratio of the star's slope to that of the A1V star atmospheric template. Since we are only concerned with the slope of the spectra longward of 1.15 μm, this correction has only been applied to the spectra that were divided by the A1V atmospheric template.

All of the reduced spectra are publicly available in electronic form[2]. Separate spectra are given for wavelengths shorter than 1.15 μm ("HR#a.fits") and longward of 1.15 μm

[2]`http://www.astro.ucla.edu/~malkan/jspec/`

("HR#b.fits").

4. Absorption Feature Identifications

We identified three absorption lines and nine blends in our stellar spectra (see Table 2). Each feature was required to satisfy the following criteria:

1. The line must be present in the spectra of many different stars within a range of surface temperatures.
2. The central wavelength must be constant in all of those spectra, to within our accuracy of one pixel = ±11.6 Å.
3. The central wavelength of the line must agree with a known transition in the appropriate stellar atmosphere model.
4. The observed line widths must be reasonable (i.e. FWHM=30–40 Å in our spectra).
5. The presence and shape of the line must not depend on the choice of atmospheric extinction template used to correct for telluric absorption.

The line identifications were based on comparison with high-resolution spectra of the Sun (Wallace et al. 1996) and the K2III star Arcturus (Hinkle and Wallace 1995). In most cases, a spectral feature in our data appears to be produced by the blending of 2 or even 3 strong lines within one of our resolution elements. The individual species creating each blend, along with their absorption feature wavelengths, are listed in columns 2 and 3 of Table 2. Where possible we have estimated which line dominates by matching the average central wavelength observed in our spectrum with the wavelength of the strongest line of the blend in the solar or Arcturus spectra. The central wavelength of the blend is given in column 4. If a feature is not a blend, but composed of a single species, then the wavelength of this single absorption feature is given in column 4. Often a change in the dominating species occurs at lower temperatures (in K and M stars) causing a shift in the blend wavelength. This new central wavelength of the blend for the cooler stars is given in parenthesis in column 4. Most lines are from neutral metals, with molecular features appearing in only the cooler stars. Notes on the species in each blend for the hotter stars are given in column 5, and any changes in the species in a blend at cooler temperatures (in K and M stars) are given in column 6. Figures 3a-e show blowups of the spectral regions with the line blends in the solar spectrum, Arcturus, and in the averages of several stars in each spectral class. As

expected, the only lines present in stars earlier than A4 were Pγ and Pβ (called Pγ and 1.28 μm respectively in Table 2).

Equivalent widths for each of the features measured are given in Table 3. Equivalent widths were measured with Gaussian fitting, and checked with the simpler direct-integration method between two "continuum" points in the IRAF SPLOT routine. Continuum points were placed along the apparent local continuum on either side of the absorption feature. The agreement between the two methods was within 1%, and the results for the Gaussian fitting are reported. Both the central wavelength and the width of the feature were left as free parameters, except in the case of the 1.33 μm blend (see below). The uncertainty in the equivalent width is typically $\sigma(\mathrm{EW}) \simeq 0.4$ Å, and, as stated, the uncertainty in the wavelength is $\sigma(\lambda) \sim 8$ Å, except where noted. In the cooler stars, the uncertainties for some of the blend equivalent width measurements are larger ($\sigma(\mathrm{EW}) = 0.8$ Å) due to the difficulty in estimating the true continuum level in a low resolution spectrum cut up by many absorption lines. Most of the lines, even the blends, are unresolved, having FWHM consistent with the instrumental resolution (28 to 32 Å). The FWHM of the Pγ and the 1.28 μm blend (which is composed primarily of Pβ) are occasionally found to be ~ 40 Å because the lines are marginally resolved. Measurements where the equivalent width measurement is particularly uncertain (where $\sigma(EW) > 0.4$ Å) due to the difficulty in determining the continuum level or a FWHM greater than the instrumental resolution are indicated with a colon in Table 3. The FWHMs of the 1.21 μm and 1.33 μm blends are greater than the instrumental resolution because their components are separated by 28 Å and 39 Å, respectively. In order to provide a more reliable measurement for the 1.33 μm blend, the FWHM was fixed at 35 Å and the core depth was measured instead of the equivalent width. The CN 0-0 index was measured from 10960 Å to 11040 Å, with continuum measured in windows on either side at 10925-10960 Å and 11040-11100 Å. This choice of wavebands is a compromise based on the need to measure as much of the absorption as possible without including noisier points at the red and blue ends. At most fifteen percent of the absorption was missed.

5. Comparison to Previous Studies at Higher Resolution

After we had completed our equivalent width measurements, Wallace et al. (2000, hereafter W2000) published results of a J-band spectroscopic survey of 88 MK standard stars, none coinciding with our sample of 105. They had a higher resolution of $R \sim 3000$, and thus did not measure all of the same blends that we identified. Many of the absorption features making up our blends could be measured individually at their higher resolution, or in some cases the individual features were not very strong and therefore were not measured

by W2000.

In order to compare our results with W2000, we degraded their digital spectra to our resolution and then measured the strongest features using our method for determining equivalent widths. As expected, the 12 features we identified in our spectra are also the strongest features in their spectra. Our measurements of these 12 features in their degraded spectra are plotted along with our data in the next section (small black circles Figure 5). The equivalent widths we measured in the degraded W2000 spectra are similar to those in our own data, and the same dependences on the effective temperature are seen. The W2000 measurements have less scatter due to the higher original resolution.

A few features (CN 0-0 index, 1.16 μm, Mg I, and 1.28 μm) were measured in both the high and low resolution spectra, making it possible to relate the measurements published by W2000 directly to what we measured. Two of the features, Mg I and 1.28 μm (known as Mg I and H Pβ in W2000) are exactly the same. Our 1.16 μm blend overlaps their Fe I feature, and we both measure the same Fe I lines. Our CN index is also contained within the CN window W2000 measured. For the 1.16 μm, Mg I, and 1.28 μm features, the equivalent widths we measured at low resolution using our technique were plotted against the high resolution measurements published by W2000 (see Figures 4a-c). It was found that the low resolution measurements have equivalent widths about 2 times the equivalent widths measured at high resolution. This increase in width at lower resolution is due to additional features included in the wider window we measured compared to that measured by W2000 in the case of the Mg I and 1.28 μm features. For the 1.16 μm feature, our window has comparable width to the W2000 feature. However, the slight displacement in wavelength causes our window to include additional features, resulting in an increased equivalent width at lower resolution. The transformations found for each of the blends are as follows, in units of angstroms:

$$EW(1.16)_{low} = 2.22 * EW(1.16)_{high} - 0.67 \tag{1.1}$$

$$EW(1.16)_{low} = 1.58 * EW(1.16)_{high} \tag{1.2}$$

$$EW(Mg\ I)_{low} = 1.95 * EW(Mg\ I)_{high} + 0.43 \tag{1.3}$$

$$EW(Mg\ I)_{low} = 2.57 * EW(Mg\ I)_{high} \tag{1.4}$$

$$EW(1.28)_{low} = 2.16 * EW(1.28)_{high} \tag{1.5}$$

The first equation given for 1.16 μm and for Mg I is the best fit line with no constraint on the y-axis intercept, and the second equation is the best fit line with a forced y-intercept of zero. For Pβ, the fits with and without forcing the intercept to zero were similar enough to just use the forced intercept fit. The linear Pearson's correlations coefficient of these transformation relations are 0.254, 0.3484, and 0.9442 for equations 1.1, 1.3, and 1.5, respectively.

Jones et al. (1996) obtained 1.16–1.22 μm intermediate-resolution spectra of 9 M dwarfs with spectral types from M2 to M6. Where our lower-resolution observations overlap with theirs, there is reasonable agreement. For example, we both find equivalent widths of the 1.17 μm blend (dominated by K I in M stars) which *increase* from 1.5 to 4 Å as the effective temperature drops from roughly 4000 to 3000 K. Our observations of the coolest M stars also appear consistent with a *decrease* from 2 to 1 Å in the equivalent width of Mg I absorption (at 1.183 μm). Although Jones et al. did not measure the Si I and 1.21 μm absorptions, they are clearly visible in their figure 1. Their spectra again confirm our observations which show that both of these absorptions drop sharply in strength at T_{eff} $\leq$3500 K. In these cool stars Fe I absorption should dominate both the 1.19 μm and 1.20 μm blends (see figure 3 of Jones et al.). Our M star observations are consistent with average equivalent widths of 1.5–2.0 Å for both of these. These line strengths agree well with the stellar atmosphere *models* in Jones et al., although their observations are systematically lower (around 1 Å or less). We could assume that the model predictions are correct. Alternatively, we could seek an explanation for why our observed equivalent widths appear higher than those of Jones et al. The fact that most of our M stars are giants, not dwarfs, could perhaps explain some of this possible discrepancy (see the Jones et al. models for varying gravity). And broad FeH absorption also inflates our measurements of the 1.20 μm blend in the coolest stars. The other possibility is that our equivalent width measurements are driven systematically higher by having 2.5 times lower spectral resolution than Jones et al.

6. Blend Analysis

6.1. Dependence on Effective Temperature

Several of the blends identified exhibit a dependence on effective temperature, and thus on spectral type. At different stellar surface temperatures, the dominating transitions that make up the blend change relative strengths, or an entirely new line may appear. The species contributing to each blend for both the hotter ($T_{eff} \geq 5000$ K) and cooler stars ($T_{eff} <$ 5000 K) are described in Table 2. This change in dominating species can cause the width and/or central wavelength of the blend to shift with temperature. The equivalent widths and FWHM of most of the blends (except for the Mg I, Si I, and 1.19 μm features) increase in the cooler stars. Plots of the equivalent width versus the effective temperature for all identified features are shown in Figures 5a-l. The 1.19 μm, 1.20 μm, 1.21 μm, 1.28 μm, and 1.33 μm blends all show systematic shifts in wavelength as well as in equivalent width (with the exception of the 1.19 μm feature which does not exhibit a change in equivalent width). The two best examples of a shift in central wavelength are shown in Figures 6a and 6b, which

plots central wavelength versus the effective temperature. For most of the blends the change in central wavelength and/or equivalent width and FWHM is due to an introduction of Ti I or CN 0-0 absorption, or a change in the relative strength of the original dominating species. Most commonly, CN 0-0 and Ti I features strengthen and C I absorption decreases as the temperature decreases. The details of the dependence of absorption on effective temperature for the individual features follows.

Pγ - This hydrogen absorption feature was measured in stars with temperatures greater than 4500 K (G9). The window measured was from 10890 Å to 10990 Å. The feature peaks in equivalent width (see Figure 5a) around 10 Å at a temperature of 10,000 K (A0V stars). In cooler stars the equivalent width drops significantly, to around 2 Å at 4500 K. For stars cooler than 4500 K, Pγ is very weak and is lost in a strong blend of CN 0-0 absorption which will be discussed below. There are only four stars hotter than 10,000 K with confident measurements, and each has a lower equivalent width than the peak.

CN 0-0 index - A strong trough of CN 0-0 absorption is present at the blue edge of our spectra in the coolest stars ($T_{eff} < 4500$ K). The window measured was from 10960 Å to 11040 Å. The CN 0-0 feature extends further to the blue, beyond the reach of our spectra. This results in our measurement underestimating the band strength, but not by more than 15%. Figure 5b shows the dependence of the equivalent width on temperature, with an increase in equivalent width with decreasing temperature.

1.16 μm blend - This feature is dominated by Si I, Fe I, and Cr I equally at the hotter temperatures, but as the temperature decreases Fe becomes more dominant and CN 0-0 is introduced. As a result of the introduction of the CN 0-0 features throughout the blend, the equivalent width increases at lower temperatures (see Figure 5c). This feature was measured from 11570 Å to 11630 Å.

1.17 μm blend - Measured from 11725 Å to 11800 Å, this feature is a blend of C I, K I, and Fe I in hotter stars. At cooler temperatures the C I lines weaken and CN 0-0 is introduced. In the coolest stars (M stars), K I (1.177 μm) dominates, with strong K I absorption at 1.169 μm also visible. A slight increase in equivalent width with decreasing temperature is seen in Figure 5d.

Mg I feature - This feature consists of a single Mg I line and was measured from 11800 Å to 11865 Å. Since the feature has no dependence on temperature and is isolated at all temperatures, no change in equivalent width or central wavelength is seen (see Figure 5e).

1.19 μm blend - Consisting primarily of two Fe I lines and some weaker C I lines at hotter temperatures, this line was measured from 11850 Å to 11910 Å. At cooler temperatures the C I absorption weakens and a Ti I line at 1.1896 μm strengthens along with several CN

0-0 features throughout the blend. The introduction of the Ti I absorption causes the central wavelength of the feature to change from 1.189 μm to 1.188 μm in cooler stars. Any dependence of the equivalent width on temperature is not detectable in our data (see Figure 5f).

1.20 μm blend - This is a blend of two Si I lines and a Fe I line in hotter stars, with the Si I line at 11987 Å the strongest of the three. This feature was measured from 11960 Å to 12000 Å. At cooler temperatures a Ti I line at 1.1977 μm is present, causing not only an increase in the width of the line at cooler temperatures (see Figure 5g), but also the wavelength shift from 1.199 μm to 1.198 μm seen in Figure 6a. In the coolest M stars, this feature changes further to be dominated by a broad trough of FeH absorption (Jones et al. 1996). Our measurements for stars with $T_{eff} \leq 3800$ K are consistent with the 1.5 Å values observed in and predicted for M dwarfs by Jones et al. (1996).

Si I feature - Measured from 12015 Å to 12070 Å, this feature consists of a single Si I absorption line. With no contamination at cooler temperatures, no change in equivalent width (see Figure 5h) or central wavelength with temperature is detected in this feature.

1.21 μm blend - This feature was measured from 12070 Å to 12150 Å. It is a blend of several Si I lines and a Mg I line. The central wavelength of the feature is shifted from 1.210 μm to 1.209 μm in cooler stars as the reddest two Si I lines weaken, while the bluer Si I and Mg I lines remain strong. CN 0-0 is also introduced throughout the blend, with the CN 0-0 on the bluer side slightly stronger than that on the redder side. This unevenness of the CN 0-0 also contributes to the shift in wavelength of the blend, as well as causing the equivalent width to increase at lower temperatures (see Figure 5i).

1.28 μm blend - This blend is dominated by Pβ at 12822 Å in hotter stars. At lower temperatures a Ti I line at 12825 Å increases in strength while the hydrogen line decreases, causing the Ti I line to be the dominating species. The feature was measured from 12760 AA to 12890 Å in stars of all temperatures. Figure 5j shows that in hotter stars this feature acts very much like the other hydrogen feature measured, Pγ, with a peak in equivalent width around 10 Å at a temperature of 10,000 K (A0V stars). In cooler stars the equivalent width deceases to around 2 Å, while for the four stars with temperatures hotter than 10,000 K it is around 5 Å. A wavelength shift is also measured in this blend (see Figure 6b). For K and M stars the wavelength shifts to the red because of the Ti I absorption feature, causing the wavelength to shift from 1.282 μm for hotter stars to 1.283 μm in the cooler stars.

1.31 μm blend - This blend consists of Si I and Al I lines and was measured from 13080 Å to 13200 Å. The Al I line at 13126 Å and the Al I line at 13180 Å are the dominating lines. Figure 5k shows a slight increase in equivalent width of this feature with decreasing

temperature.

1.33 μm blend - This blend is made up of several species with Si I and Fe I lines dominating. The window in which this feature was measured is from 13250 Å to 13335 Å. In cooler stars the Fe I and Ca I lines weaken and the Mn I lines strengthen. This change in dominating species causes a wavelength shift from 1.332 μm to 1.331 μm in cooler stars. At the lowest stellar temperatures, a band of H_2O absorption (Jones et al. 1996) cuts into the red side of this blend, making it very difficult to measure. At cooler temperatures the equivalent width of this feature increases slightly (see Figure 5l).

6.2. Dependence on Gravity

Along with a dependence on the effective temperature, several of the blends identified have a dependence on the luminosity class of the star and thus on the gravity. This is most noticeable in the F through K spectral classes where we have reasonably large samples of dwarfs, giants and supergiants. The strongest case is the Mg I line which has a larger equivalent width for dwarfs (luminosity classes IV and V) than for giants (luminosity classes I, II, and III) at a given effective temperature (see Figure 5e). The 1.16 μm blend exhibits the opposite dependence on gravity, having a larger equivalent width for giants (see Figure 5c). 1.31 μm has the same dependence, but to a lesser degree. None of the other blends show much of a dependence on gravity.

6.3. Dependence on Metallicity

Fifteen of the stars in our sample are known from high resolution optical spectroscopy to have high or low metal abundances (see logarithmic metallicity values in the last column of Table 1). The high and low metallicity stars are shown in Figures 5 and 6, with high abundance stars defined as $[Fe/H] > 0.0$ and low abundance as $[Fe/H] < -0.3$. For a given temperature, those stars with high (low) metallicity tend to have enhanced (diminished) equivalent width for some metal absorption blends, relative to the majority of normal stars (presumed to have solar, Population I abundances). The strongest case is the 1.19 μm blend where ΔEW/Δlog[Fe/H] ~ 2. The 1.28 μm blend also has a positive dependence on metallicity, which is surprising, since the feature is dominated by hydrogen. The dependence might be due to the introduction of Ti I absorption at lower temperatures. Some of the blends (Pγ, 1.17 μm, 1.20 μm, and 1.21 μm) have no apparent dependence on metallicity within the accuracy of our measurements.

7. IR Stellar Spectral Classification

7.1. Temperature Indicator

The blends most sensitive to the effective temperature are 1.28 μm and 1.31 μm, as well as the CN index. Hotter stars have higher 1.28 μm equivalent widths, while 1.31 μm and the CN index have the opposite temperature dependence. Using these relationships between equivalent width and effective temperature, it is possible to estimate a given star's effective temperature based on a measurement of the equivalent width of one or two absorption features. The dependence of 1.31 μm is not as strong as that of 1.28 μm. However, 1.28 μm is only useful for effective temperatures between 5500 K and 9500 K, due to the addition of the Ti I line at these lower temperatures, and the turndown in the equivalent width for spectral types earlier than A0. Since the CN 0-0 absorption only occurs in the coolest stars, the CN index is useful as a temperature indicator for stars with effective temperatures less than 5500 K. If CN 0-0 absorption is detected, the star has an effective temperature less than 5500 K; if it is absent then the 1.28 μm blend can be measured, and a temperature greater than 5500 K will be found. Using the equivalent width of the 1.28 μm blend it is possible to estimate an effective temperature to within 1600 K, while using the CN index will give an effective temperature to within 1300 K. To quantify these dependencies on effective temperature the following relationships are used:

$$T(1.28) = 1139 * EW(1.28) + 2211 \tag{2}$$

$$T(CN) = -677 * EW(CN) + 5905 \tag{3}$$

Figure 7a shows the 1.28 μm blend equivalent width versus the published temperatures for all stars with 5500 < T < 9500 K, except those stars with uncertain equivalent width measurements (σ(EW) > 0.4 Å) or high/low metallicity (see § 6.3), and the fit given by Equation 2. The same plot of the CN 0-0 index equivalent width for stars with T < 6000 K is given with Figure 7b, with the fit given by Equation 3 shown.

Another method to determine the effective temperature of a star is to use the spectral shape. As explained in §3, the slope of the final stellar spectrum is a result of the slope of the star divided by the slope of the A star atmospheric template. The slope of the spectra are found to be dependent on the effective temperature with a greater, positive (with respect to wavelength) slope for stars with cooler effective temperatures. For an A star, which intrinsically has a slope close to that of a 10,000 K black body, this *differential* slope is then measured to be about zero, while for stars with cooler effective temperatures the slope increases. The slope of these stellar spectra ratios were determined by fitting a power law ($F_\lambda = C\lambda^\alpha$) to the final ratio spectrum between 1.14 μm to 1.34 μm. It was found that the

differential slope α_{diff} depends on the effective temperature in the following way (see Figure 8):

$$T(slope) = -2325 * \alpha_{diff} + 9574 \quad (4)$$

This relationship holds for temperatures less than 13500 K. Using the slope of the ratio of the stellar spectrum to the A star atmospheric template, it is possible to determine the effective temperature of a star to within 2500 K. The temperature determined from the differential slope of the spectrum agrees with the temperature given by the equivalent width to within 2000 K (see Figure 9).

7.2. Surface Gravity Indicator

As discussed earlier, Mg I, 1.16 μm, and Pγ are particularly sensitive to the luminosity class of the star. To quantify this dependence, the following equation was used to make a fit of one blend plotted against another:

$$EW(1st\ blend) = constant1 + constant2 * EW(2nd\ blend) + constant3 * Lum.\ Class \quad (5)$$

where the luminosity class is represented by I=1, II=2, etc. The form of Equation 5 is not necessarily the best representation of the relationship between luminosity class and equivalent width, but was chosen for its simplicity. The dominant term, as expected, is the equivalent width of the 2nd line, but for those lines which have a strong dependence on the surface gravity the third term is significant. Those stars with known high or low metallicities were not included in the fit, nor were stars with uncertain equivalent width measurements (σ(EW) > 0.4 Å). When fitting the equivalent width of Mg I versus the equivalent width of any of the other blends, the Mg I luminosity class coefficient is large and positive, indicating that dwarfs have higher equivalent widths than giants of similar effective temperature. A similar result was found for Pγ, but the coefficient is smaller than the one found for Mg I. 1.16 μm has the opposite characteristic, having a large, negative coefficient multiplying the luminosity class in Equation 4. This indicates that 1.16 μm is a good indicator of giants, having a higher equivalent width for giants than it does for dwarfs. The ratio of the equivalent width of Mg I to the equivalent width of the 1.16 μm blend can therefore be used as an indicator of the luminosity to within one luminosity class, as illustrated in Figure 10. The greater the ratio, the lower the luminosity class (see Figure 10), or, quantitatively stated:

$$EW(1.16) = 2.696 * EW(Mg\ I) - 0.73 * Lum.\ Class \quad (6)$$

This fit was done with all luminosity classes weighted equally. Thus, the above relationship is not the best fit to each luminosity class individually, but rather to an average of the luminosity classes.

7.3. Classification Scheme

As has been illustrated above, the ratio of the equivalent widths of Mg I to 1.16 μm is an indicator of the luminosity class, while the equivalent width of either 1.28 μm or the CN index can be used as an indicator of the effective temperature. Also, the slope of the continuum can be used to estimate the effective temperature. Combining this information, a classification can be made of a star to within three subclasses based on easily measured quantities. Of course, the slope of a star is not completely reddening independent. Using the temperature measurement based on the equivalent width of the 1.28 μm bland or CN index one could use the observed slope to deduce independently the approximate reddening of a given star.

8. Conclusions

The principal result of our observations of hot stars is that, at least at our spectral resolution, it is safe to approximate their spectra as featureless blackbodies, after removing the Pβ and Pγ absorption lines. Thus these stars are useful for measuring the atmospheric extinction.

Even at the low resolution of this study, nine blends and three lines were identified. As expected, the most important stellar property controlling the absorption line strengths we measured is the effective stellar surface temperature. The strength of the Paschen lines peaks at a maximum equivalent width of 10 Å at A0 and declines at higher and lower temperatures. The neutral metal lines are not strong until later than A7, and their strength increases in cooler stars. The most noticeable change in the spectra as the temperature decreases is the increase of CN 0-0 and Ti I lines and the relative decrease of C lines. There is, however, significant cosmic scatter (i.e., larger than observational) in the line strengths for stars of a given surface temperature. A dependence on metallicity was also found, particularly for the 1.19 μm and 1.28 μm blends, with stars of higher (lower) metallicity having elevated (diminished) equivalent widths.

The classification of a star, even in the presence of strong reddening, is possible by obtaining the equivalent widths of four blends, or the equivalent widths of two blends and the slope of the stellar spectrum. The ratio of Mg I (or Pγ, though it is less reliable) to 1.16 μm indicates the surface gravity of the star, with a higher ratio for lower surface gravity stars. The temperature can be estimated using the equivalent width of the 1.28 μm blend or the CN index, or alternatively the slope of the spectrum can be used. Measuring these temperature- and gravity-sensitive features in integrated spectra of composite stellar popu-

lations (in star clusters or galaxies for example) can therefore provide constraints on the age and other astrophysical properties of the system.

We thank Don Figer for help with an IRAF script for spectroscopic data reduction.

REFERENCES

Cayrel de Strobel, G. Soubiran, C., Friel, E. D., Ralite, N., Francois, P. 1997, A&AS, 124, 299

Fanson, J. L. 1998, SPIE, 3356, 478

Figer, Donald F., McLean, Ian S., Morris, Mark 1999, ApJ, 514, 202

Hicks, E. K., Malkan, M. A., Teplitz, H. I., Sugai, H., Guichard, J. 2000, AAS, 197, 4408

Hinkle, K., Wallace, L., Livingston, W., 1995, PASP, 107, 1042

Jones, H. R. A., Longmore, A. J., Allard, F., and Hauschildt, P. H. 1996, MNRAS, 280, 77

Lancon, A. and Rocca-Volmerange, B. 1992, A&AS, 96, 593

McLean, Ian S., Macintosh, Bruce A., Liu, Tim, Casement, L. S., Figer, Donald F., Lacayanga, Fred, Larson, Sam, Teplitz, Harry, Silverstone, Murray, Becklin, Eric E. 1994 SPIE, 2198, 457

McLean, I. S., 1994, in *Infrared Astronomy with Arrays: the Next Generation*, ed. McLean, I.S. (Kluwer)

McLean, I. S., et al. 1998, Proc. SPIE, 3354, 566

McLean, I. S., et al. 2000, ApJ, 533, L45

Mouhcine, M., Lancon, A. 2001 ApSSS, 277, 485

Nesterov, V. V., et al. 1995, ApJS, 110, 367

Stockman, H.S., 1997, ed., "Next Generation Space Telescope: Visiting a Time When Galaxies Were Young", (AURA, Inc.: Baltimore)

Sugai, H., Malkan, M. A., Ward, M. J., Davies, R. I., McLean, I. S. 1997, ApJ, 481, 186

Wallace, L., Livingston, W., Hinkle, K., Bernath, P., 1996, ApJS, 106, 165

Wallace, Lloyd, Meyer, Michael R., Hinkle, Kenneth, Edwards, Suzan 2000, ApJ, 535, 325

Wallace, Lloyd and Hinkle, Kenneth 1996, ApJS, 107, 312

Table 1. J-Band Atlas Stars

HR #	Type	Teff(K)	Date Obs.	[Fe/H][a]	HR #	Type	Teff(K)	Date Obs.	[Fe/H][a]
81	A0V	9480	1999 Sep 19	···	4886	A7V	7930	1996 Mar 14	···
106	K5III	3980	1996 Aug 26	···	4900	A7III	7650	1996 Mar 14	···
207	G0Ib	5510	1999 Sep 19	···	4943	B9V	10700	1996 Mar 14	···
217	F8V	6135	1996 Aug 26	···	4967	B7III	13200	1996 Mar 14	···
225	F8V	6135	1994 Dec 16	···	5191	B3V	19000	1999 Sep 18	···
232	A3V	8595	1996 Aug 26	···	5322	F9V	6035	1996 Mar 13	0.20
246	A2V	8810	1996 Aug 26	···	5747	F0Vp	7020	1999 Sep 17	0.825
601	M2III	3710	1999 Sep 19	···	5770	B9V	10700	1997 Mar 30	···
611	K5Iab	3850	1996 Aug 26	···	6088	A3V	8595	1997 Oct 13	···
617	K2III	4260	1999 Sep 18	-0.258	6156	A1V	9150	1996 Aug 25	···
690	F7Ib	6370	1999 Sep 19	···	6466	G0III	5910	1999 Sep 18	···
695	G2V	5830	1996 Aug 26	-0.10	6518	K0V	5240	1999 Sep 18	···
719	K0III	4810	1999 Sep 17	···	6598	F9V	6035	1997 Oct 13	-0.39
747	K5Iab	3850	1999 Sep 18	···	6604	F5II	6640	1999 Sep 17	0.55
753	K3V	4790	1999 Sep 18	···	6685	F2Ibe	7170	1999 Sep 17	-0.41
867	M6III	3250	1999 Sep 19	···	6985	F5III	6470	1999 Sep 18	0.10
921	M4II	2980	1999 Sep 19	0.05	7139	M4III	3560	1999 Sep 17	···
940	M0III	3820	1999 Sep 18	···	7345	G8V	5430	1999 Sep 18	···
1542	O9.5I	3250	1994 Dec 17 0	0.30	7373	G8IV	5430	1999 Sep 18	0.38
1544	A1V	9150	1997 Oct 13	···	7384	A0V	9480	1999 Sep 17	···
1562	M1III	3780	1999 Sep 18	···	7471	B3III	17100	1999 Sep 19	···
1683	A0V	9480	1995 Jan 19	···	7475	K4Ib	3990	1999 Sep 17	···
1684	K5III	3980	1997 Oct 13	-0.11	7563	F0III	7150	1999 Sep 18	···
1703	M0V	3800	1999 Sep 19	···	7589	O9.5I	32500	1996 Mar 14	···
1988	G4V	5740	1997 Oct 13	···	7596	A0III	10100	1999 Sep 18	···
2007	G4V	5740	1997 Oct 15	···	7696	M3III	3630	1999 Sep 18	···
2034	A0V	9480	1999 Sep 19	···	7776	K0:II:+AII	4420	1999 Sep 17	0.62
2208	G2V	5830	1997 Oct 14	···	7800	K7III	3920	1999 Sep 18	···
2285	A4V	8375	1995 Jan 19	···	8143	B9Iab	10500	1997 Oct 12	···
2375	A3V	8595	1997 Oct 14	···	8149	K5III	3980	1994 Dec 16	···
2401	F8V	6135	1995 Dec 9	···	8279	B2Ib	17800	1997 Mar 30	-0.33
3257	A2V	8810	1994 Dec 17	···	8328	A1V	9150	1997 Oct 12	···
3436	G8III	4960	1995 Jan 19	···	8334	A2Iab	9080	1999 Sep 18	···
3592	A3V	8595	1997 Mar 29	···	8345	A2Ib	9080	1999 Sep 18	···
3608	A2V	8810	1994 Dec 16	···	8518	K4V	4560	1996 Mar 13	0.3
3719	A5V	8160	1996 Mar 9	···	8631	G4V	5740	1994 Dec 15	···
3750	G2V	5830	1994 Dec 17	-0.31	8692	G4Ib	4900	1999 Sep 19	···

Table 1—Continued

HR #	Type	Teff(K)	Date Obs.	[Fe/H][a]	HR #	Type	Teff(K)	Date Obs.	[Fe/H][a]
3881	G0.5Va	5860	1995 Jan 18	0.0	8718	F5II	6640	1999 Sep 19	0.045
3998	F7V	6390	1995 Jan 18	0.0	8726	K5Ib	3850	1999 Sep 19	0.015
4012	F9V	6035	1995 Jan 20	0.115	8738	A1V	9150	1994 Dec 15	···
4026	A8III	7320	1994 Dec 17	···	8826	A5Vn	8160	1997 Oct 13	···
4051	F9V	6035	1996 Mar 9	···	8852	G9III:Fe2III	4890	1999 Sep 19	-0.382
4215	A1V	9150	1995 Jan 19	···	9010	K3II	4130	1999 Sep 19	···
4412	F7V	6240	1996 Mar 9	···	9053	G8Ib	4590	1999 Sep 19	···
4439	F8V	6135	1994 Dec 16	···	9066	M7IIIe	3080	1999 Sep 19	···
4454	A5V	8160	1995 Jan 18	···	9099	M4III	3560	1999 Sep 19	···
4632	A4V	8375	1996 Mar 9	···	HD10986	K5III	3980	1996 Aug 26	···
4660	A3V	8595	1994 Dec 17	···	HD11469	M3.5I	3090	1996 Aug 26	···
4663	A3V	8595	1997 Mar 30	···	HD18881	A0V	9480	1996 Oct 26	···
4708	F8V	6135	1995 Jan 18	···	HD36395	M1.5V	3600	1999 Sep 18	0.60
4767	F9V	6035	1994 Dec 17	-0.11	HD162208	A0V	9480	1996 Aug 25	···
4861	A1V	9150	1996 Mar 14	···	HD184314	K5V	4340	1996 Aug 25	···
4875	A3V	8595	1996 Mar 14	···					

[a]Cayrel de Strobel, G., et al. 1997, A&AS, 124, 299

Table 2. Spectral Features Identified

	Dominant Features				
Name	Element(s)	λ(μm)	Blend λ (K-M λ)[a]	Comments	Cool Stars
P γ	H I		1.0942		Not present in K and M stars
CN 0-0 index	CN		1.0960-1.1040		Present in $T_{eff} \leq 5500$ K
1.16	Si I/Si I/Fe I	1.1595	1.1600		Fe strongest, CN 0-0
	Fe I/Cr I/Si I	1.1612			present
1.17	C I (3 lines)	1.1753	1.1775		C weaker, CN 0-0 present
	K I/K I/C I/Fe I	1.1780			K I in late M
Mg I	Mg I		1.1831		
1.19	Fe I	1.1886	1.1886 (1.1875)	Several C I lines	C weaker, Ti I(1.1896)
	Fe I	1.1887			present, CN 0-0 present
1.20	Fe I	1.1976	1.1985 (1.1980)	Si I(1.1987) strongest	Ti I(1.1977) present
	Si I	1.1987			FeH trough in late M
	Si I	1.1995			
Si I	Si I		1.2034		
1.21	Si I	1.2086	1.2100 (1.2090)	Si I(1.2086) and	Si I(1.2106) weaker
	Mg I	1.2087		Mg I(1.2106) strongest	
	Si I	1.2106			
	Si I	1.2114			
1.28	H I		1.2822 (1.2830)		Ti I(1.2825) present
1.31	Si I	1.3105	1.3145	Al I(1.3126) and	
	Al I	1.3126		Si I(1.3180) strongest	
	Al I	1.3154			
	Si I	1.3180			
1.33	Si I	1.3291	1.3320 (1.3310)	Si I(1.3291),Si I(1.3313)	Fe and Ca lines weaker
	Si I	1.3313		and Fe I/Si I(1.3330)	and Mn lines strengther
	Fe I/Si I	1.3330		strongest	H_2O absn in late M

[a]If a shift in central wavelength with change in temperature is present, then the central wavelength for cooler stars (K and M stars) is given in parenthesis.

Table 3. Equivalent Widths of Each Line/Blend

HR #	ST	Pγ	CN 0-0	1.16	1.17	Mg I	1.19	1.20	Si I	1.21	1.28	1.31	1.33 [c]
1542	O9.5I	2.61[b]	···	···	···	···	···	···	···	···	0.61	···	···
7589	O9.5I	13.91	···	···	···	···	···	···	···	···	1.84	···	···
8279	B2Ib	2.67	···	···	···	···	···	···	···	···	7.39:[b]	···	···
5191	B3	6.24	···	···	···	···	···	···	···	···	2.88	···	···
7471	B3III	9.08:[b]	···	···	···	···	···	···	···	···	7.46:[b]	···	···
4967	B7III	6.16	···	···	···	···	···	···	···	···	5.79	···	···
4943	B9V	8.77	···	···	···	···	···	···	···	···	7.44:	···	···
5770	B9V	21.62:	···	···	···	···	···	···	···	···	8.06:	···	···
8143	B9Iab	3.09	···	···	···	···	···	···	···	···	4.27[b]	···	···
1683	A0V	7.09	···	···	···	···	···	···	···	···	8.34:	···	···
81	A0V	7.75	···	···	···	···	···	···	···	···	7.13	···	···
HD18881	A0V	7.96	···	···	···	···	···	···	···	···	7.54	···	···
HD162208	A0V	7.05	···	···	···	···	···	···	···	···	7.68	···	···
7384	A0V	9.76:	···	···	···	···	···	···	···	···	13.02:	···	···
2034	A0V	7.55:	···	···	···	···	···	···	···	···	11.89:[b]	···	···
7596	A0III	10.49:	···	···	···	···	···	···	···	···	10.62:[b]	···	···
4215	A1V	7.18	···	···	···	···	···	···	···	···	7.44:	···	···
4861	A1V	6.27	···	···	···	···	···	···	···	···	7.07	···	···
8738	A1V	7.27	···	···	···	···	···	···	···	···	8.63	···	···
6156	A1V	2.10[a]	···	···	···	···	···	···	···	···	7.08:	···	···
8328	A1V	8.78:[b]	···	···	···	···	···	···	···	···	6.04:	···	···
1544	A1V	7.86	···	···	···	···	···	···	···	···	6.04:	···	···
3608	A2V	9.46	···	···	···	···	···	···	···	···	6.41	···	···
3257	A2V	6.40	···	···	···	···	···	···	···	···	6.56	···	···
246	A2V	4.97	···	···	···	···	···	···	···	···	4.50	···	···
8334	A2Iab	2.30	···	···	···	···	···	···	···	···	4.45[b]	···	···
8345	A2Ib	2.23[b]	···	···	···	···	···	···	···	···	3.94	···	···
4663	A3V	13.11:	···	···	···	···	···	···	···	···	9.02:	···	···
4875	A3V	6.87	···	···	···	···	···	···	···	···	6.55	···	···
4660	A3V	6.51	···	···	···	···	···	···	···	···	5.00	···	···
6088	A3V	5.86	···	···	···	···	···	···	···	···	7.34:	···	···
2375	A3V	7.55	···	···	···	···	···	···	···	···	7.41:	···	···
232	A3V	5.95[b]	···	···	···	···	···	···	···	···	6.75	···	···
3592	A3V	6.35	···	···	···	···	···	···	···	···	9.87:	···	···
2285	A4V	5.76	···	···	···	···	···	···	···	···	7.04:	···	···
4632	A4V	5.63	···	1.42	1.12	2.17	1.63	1.23	1.18	1.14:	7.26	1.38	2.43
4454	A5V	5.09	···	···	···	···	···	···	···	···	6.17	···	···
3719	A5V	5.28	···	1.51	1.03	3.79:	1.33	1.41[a]	1.37	1.41[a]	7.76	1.01	2.30

Table 3—Continued

HR #	ST	Pγ	CN 0-0	1.16	1.17	Mg I	1.19	1.20	Si I	1.21	1.28	1.31	1.33 [c]
8826	A5Vn	6.17	···	···	···	···	···	···	···	···	6.00	···	···
4886	A7V	4.18	···	1.03	1.41[a]	1.34:	1.50:	0.79:	1.13	0.53	5.72	1.08	2.02
4900	A7III	4.72	···	1.74	1.18	1.41[a]	1.41[a]	1.63	1.93	1.16	5.28	0.56	1.30:
4026	A8III	7.45	···	1.79:	0.91	2.85	1.89	1.59	1.75	1.02:	7.67	1.01	5.43:
5747	F0Vp	5.35	···	6.40:	1.09	3.65	3.22	1.59	2.41	0.60	14.73:	4.17	8.14
7563	F0III	2.87	···	2.61	1.57	2.67	1.97	1.51	1.23	1.41[a]	7.86	2.63	3.74
6685	F2Ibe	2.20:[b]	···	1.37	3.11[b]	1.03	1.18	0.58	0.96	0.97	4.41:	1.90	3.48
6604	F5II	3.23	···	1.08	4.14:[b]	2.93	4.30	1.70	2.26	1.16	11.68:	4.05	6.06
8718	F5II	7.19:	···	4.35	1.11	0.85	1.75	0.98	1.48[b]	0.31	7.45:[b]	1.32[b]	1.16:
6985	F5III	2.96	···	3.31:[b]	0.84	1.57	5.44:	1.28	0.81	1.10	7.70:[b]	1.86[b]	3.10
3998	F7V	1.77	···	1.91	1.01	1.65:	0.90	1.12	0.92	1.61:	3.88	1.35	2.61
4412	F7V	1.87	···	1.77	0.84	1.49	1.07	1.07	1.05	1.45	4.30	1.29	3.29
690	F7Ib	4.64:[b]	···	2.09:	2.17	1.04	1.00	1.57	0.84	1.41[a]	4.97[b]	1.30[b]	0.84:
4439	F8V	1.71	···	2.03	0.86	3.66:	1.75	1.02	1.25	0.81	2.42	1.56	4.87
225	F8V	1.45	···	1.31	1.41[a]	1.53	1.69	1.40	0.68	1.41[a]	2.48	0.81	2.94
4708	F8V	1.79	···	1.76	0.95	1.89	1.30	1.05	1.38	1.61	3.29	1.08:	2.73
2401	F8V	0.97	···	2.29:	1.09	1.83	1.23	0.74	1.63	1.87:	2.94	0.65	1.32
217	F8V	2.44:[b]	···	1.62:	0.97	1.06	1.10	0.88	1.01	0.80	3.19	1.47	1.63
4012	F9V	1.42	···	1.28	1.25	1.03	0.84	0.64	0.54	0.94	3.20	1.07:	0.93
5322	F9V	2.52:	···	1.39:	1.41[a]	1.85	2.03	3.53:	1.71:	1.61:	2.99	1.61	3.04
4051	F9V	2.38	···	2.76	1.27	1.41[a]	1.42	0.76	1.28	1.24	3.33	1.58	2.79
4767	F9V	1.80	···	1.68:	0.98	2.41	1.51	1.09	1.44	0.98	2.96	1.16	3.43
6598	F9V	1.12	···	0.47:	0.29	1.12	0.31:	1.25:	0.92:	0.59:[b]	1.87	0.36:	0.92
207	G0Ib	6.41:[b]	-0.42	3.08[b]	1.26	0.85	0.52	1.71[b]	0.97[b]	1.41[a]	4.16:[b]	1.77[b]	3.04
6466	G0III	9.69:[b]	-0.95	2.33	1.00	2.19[b]	1.93	1.30	0.79	1.41[a]	4.00:[b]	1.10[b]	1.40:
3881	G0.5Va	0.84	···	1.77	0.40	1.17:	1.19	1.08	1.48	1.60:	2.29	1.31	2.39
695	G2V	0.52:	-0.03	1.27	0.23:	1.68:	1.09	1.41	1.41[a]	0.45:	2.45	0.86:	2.75
3750	G2V	1.39:	3.92	1.46	2.46:	3.45:	1.97	0.98	1.61	0.91	1.07	0.95	4.59
2208	G2V	1.12	0.21	1.99	0.87:	2.28	1.33	2.68:	1.53	1.72	2.29	1.41[a]	···
8631	G4V	0.85:	0.62	1.77	2.47:	2.58	1.57	1.46	1.09	2.46:	1.15	1.12	5.37:
1988	G4V	1.74	···	1.45	1.03:	0.89	1.35	1.05	0.88	1.13:	1.92	0.29:	1.08
2007	G4V	1.95:	-3.18	0.63:[b]	0.83	1.54	0.88:	0.90	0.60	0.69:	2.06	0.51	3.28
8692	G4Ib	16.80:[b]	3.66	4.77:[b]	1.26	1.27[b]	2.28	3.10	2.36[b]	1.36	2.77:	2.16[b]	4.58
7345	G8V	4.45	-1.56	2.60:[b]	1.10	1.84[b]	2.43	2.32	1.41[b]	1.58	4.10[b]	2.51[b]	2.80
9053	G8Ib	17.63:[b]	···	3.66:[b]	1.29	1.11[b]	1.98	2.18	0.93[b]	1.41	3.57:	1.96[b]	3.38
3436	G8III	1.65:	···	1.41[a]	0.91	1.12	0.61	0.98	0.98[b]	0.98	1.43	0.49:[b]	···
7373	G8IV	8.13:[b]	-0.62	3.33:	2.63:[b]	2.05	2.84	1.86	2.11	1.22	4.94:	2.93	5.50
8852	G9III:Fe2	3.63[b]	-0.07	4.17	2.00	3.08	3.37	2.29	1.42	1.82:	4.27:[b]	3.06	6.13

Table 3—Continued

HR #	ST	Pγ	CN 0-0	1.16	1.17	Mg I	1.19	1.20	Si I	1.21	1.28	1.31	1.33 [c]
6518	K0V	···	2.17	2.01	0.79	2.32[b]	0.89	1.98	1.76[b]	1.15	3.08:[b]	2.31[b]	3.38
7776	K0:II:+A5:N	···	54.99:	9.01:	2.04	3.49	7.85:[b]	1.84	2.84	0.74	3.62	5.83	15.22
719	K0III	···	0.95	4.51	0.92	3.10	4.43	1.56	2.26	0.99	4.63:	4.17	12.24
617	K2III	···	1.67	4.38	0.94	3.54	0.95	1.75	2.42	0.51	2.48	5.17	8.78
753	K3V	···	5.92:	3.19	1.11	2.71	3.43:	1.44	1.44	1.41[a]	3.66:	4.31	6.26
9010	K3IIb	···	6.94	5.50:	1.55	3.10[b]	1.32[b]	1.25	1.09[b]	0.85	3.54:	2.06[b]	3.49
8518	K4V	···	2.54	1.98	1.50	3.14:	1.60	1.25:	1.21	1.40	0.61:	2.62:	4.73
7475	K4Ib	···	7.48	6.22	1.66	3.90	4.49	2.81	3.54	1.41[a]	5.25:	4.76	8.36
HD184314	K5V	···	1.61	2.90	1.45	2.50	2.21	1.41	1.73	1.92:	1.46	0.96	1.64
HD10986	K5III	···	6.19	1.90	1.42	2.36	2.32	1.39	0.74	2.04	1.00	1.97	1.41
106	K5III	···	3.96	1.84	1.13:	1.41[a]	1.22	1.22:	0.67	1.41[a]	1.37	1.41:	2.00
1684	K5III	···	3.81	2.41:	1.07	1.22	1.28	1.37	0.28:	0.72	1.33	0.99	2.07
8149	K5III	···	1.69	1.87	2.61:	1.93	1.87	0.79	0.55	0.84	1.68	0.78	1.76
747	K5Iab	···	4.24	1.41[a]	1.55	1.07	1.41[a]	1.09:	0.81	1.69:	1.18	1.32	1.30
611	K5Iab	···	3.21	2.30	1.40	1.84	2.34	1.40	1.19	2.18	4.00	1.44	2.10
8726	K5Ib	···	4.82	7.50	1.80	1.35	2.22	4.15:	1.11	1.60:[b]	5.53:[b]	4.09	4.53
7800	K7III	···	2.00	2.56:	3.78:	0.33	0.65	0.60	0.78	1.41[a]	3.49:[b]	1.44	3.13
1703	M0V	···	4.50	3.37:	2.56:	0.36	0.35	0.50	0.58	1.41[a]	3.62:[b]	1.20	3.05
940	M0III	···	1.13	5.27	1.90	2.73	2.75	1.21	1.13	1.41[a]	1.27	5.74:	6.15
1562	M1III	···	2.30	3.36	1.47	2.43	2.32	1.71	1.47	1.52	2.81	3.44	6.03
HD36395	M1.5V	···	3.35	3.41[b]	1.72	3.30:	3.04	1.97	2.64	0.98	2.46	5.12	8.48
601	M2III	···	1.86	8.13:	1.03	1.91	1.06	1.60	0.75	1.41[a]	2.55:	2.22:	···
7696	M3III	···	0.64	1.69	4.42:	0.67	1.07	2.87:	1.14	1.41[a]	2.62:	1.66	1.38
HD11469	M3.5I	···	3.98	2.21	1.96:	1.10	1.59	1.25:	1.41[a]	1.33	1.65	1.41[a]	0.37
921	M4II	···	1.70	2.40:	0.99	1.08	0.95	···	1.41[a]	0.69	3.15:	1.41[a]	···
7139	M4III	···	58.44:	8.86	3.37[b]	2.80	4.59	3.01	3.72	1.04	5.20:	5.13	11.83
9099	M4III	···	3.49	3.99[b]	1.79	2.93:[b]	3.01[b]	2.65[b]	1.20[b]	1.56	3.15[b]	3.16[b]	···
867	M6III	···	8.07:	3.43:	1.91:	1.47:[b]	1.99	2.63:	0.38	0.65	4.27:[b]	3.50:[b]	0.71
9066	M7IIIe	···	2.63	1.13[b]	2.62	1.41[a]	5.22:	2.27:[b]	0.33[b]	1.38	3.34	3.23[b]	5.14

[a]Three sigma upper limit

[b]Wavelength off by more than 8 Å

[c]The FWHM was fixed at 35 Å and the cored depth is reported rather than equivalent width.

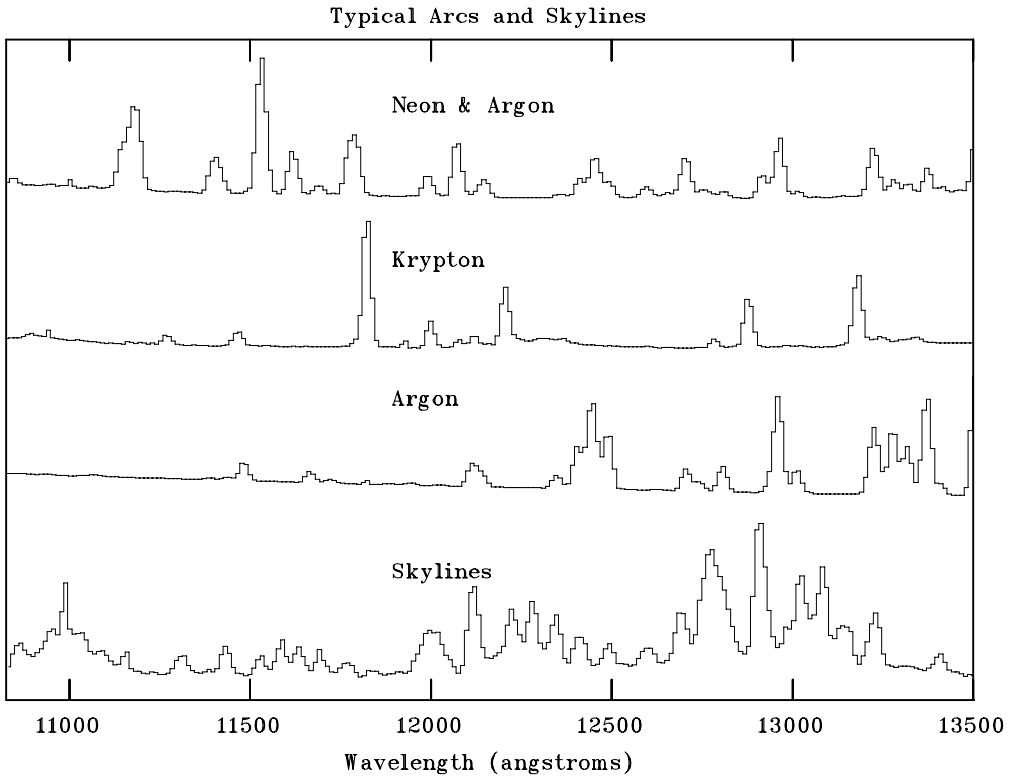

Fig. 1.— Arc lamp used for calibrating data. Sky lines were used when no arc lamp was available. Each of the spectra have been scaled to unity and an arbitrary additive constant has been added to the fluxes on the vertical scale.

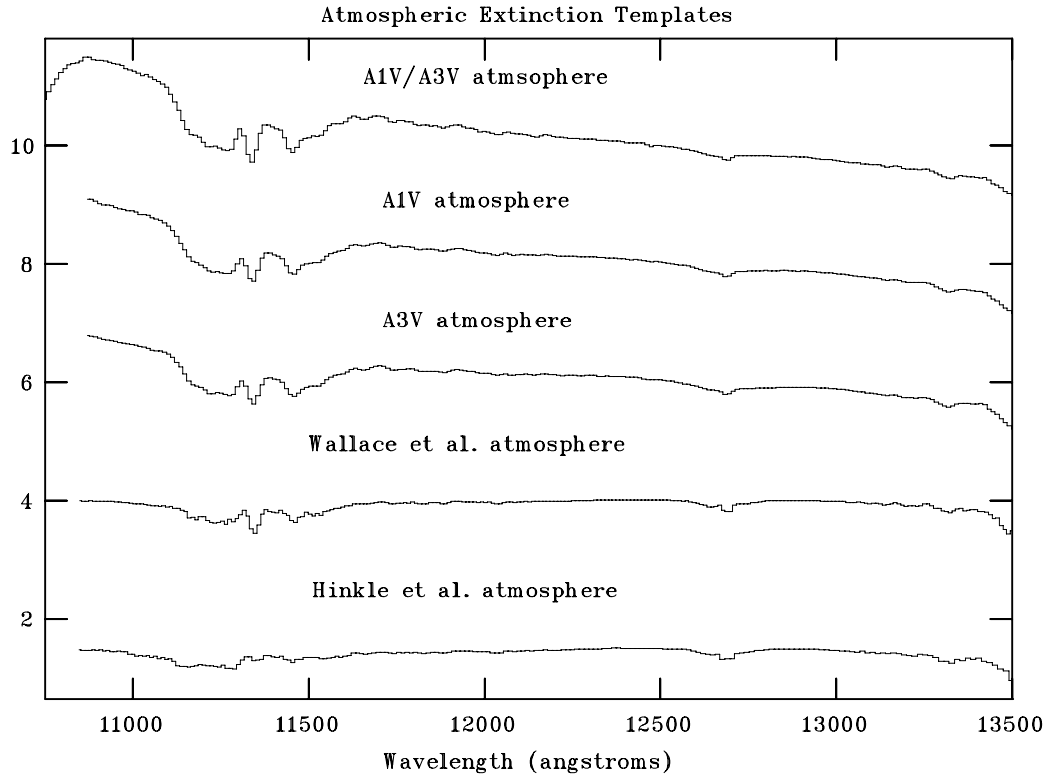

Fig. 2.— Atmosphere extinction spectra. The A1V/A3V atmosphere spectrum was used for the region between 1.07 μm and 1.10 μm, while the A1V atmosphere spectrum was used for the region between 1.15 μm and 1.35 μm. The other three atmosphere spectra were also tried to check that the absorption features identified were not dependent on the atmosphere spectra used. The atmospheric template used for atmosphere correction in the solar spectrum and Arcturus spectrum are those published by Wallace et al. (1996) and Hinkle et al. (1995), respectively. The spectra have been scaled to unity and shifted vertically by 2.0.

Fig. 3.— Blowup windows of each feature identified with spectra of several stars of similar spectral type(s) averaged together. The spectral types included in the averaged spectrum are given to the right of the spectrum and the number of stars averaged together is in parentheses. Also plotted are the high resolution solar and Arcturus spectra, labeled Sun(H) and Arct.(H) respectively, and the same spectra degraded to match our resolution, labeled Sun(L) and Arct.(L) respectively. The horizontal lines indicate the window in which the labeled feature was measured. The larger vertical dashed lines mark the centers of the features. For those feature for which a wavelength shift was present, the smaller vertical dached line marks the center of the feature in hotter stars (earlier than K) and the larger dashed line is the center of the feature for cooler stars (K and M stars). The features shown in each figure are as follows: (a) Paschen γ (1.0942 μm) and CN index, (b) 1.16 μm, 1.17 μm and Mg I (1.1831 μm), (c) 1.19 μm, 1.20 μm, Si I (1.2034 μm), and 1.21 μm, (d) 1.28 μm, and (e) 1.31 μm and 1.33 μm. All spectra have been scaled to 2 and shifted by an arbitrary additive constant along the vertical scale. The emission features seen in the Arcturus spectrum are due to poor sky subtraction, as are apparent absorption features with FWHM < 0.1 Å, which appear as spikes of one line width in our plots.

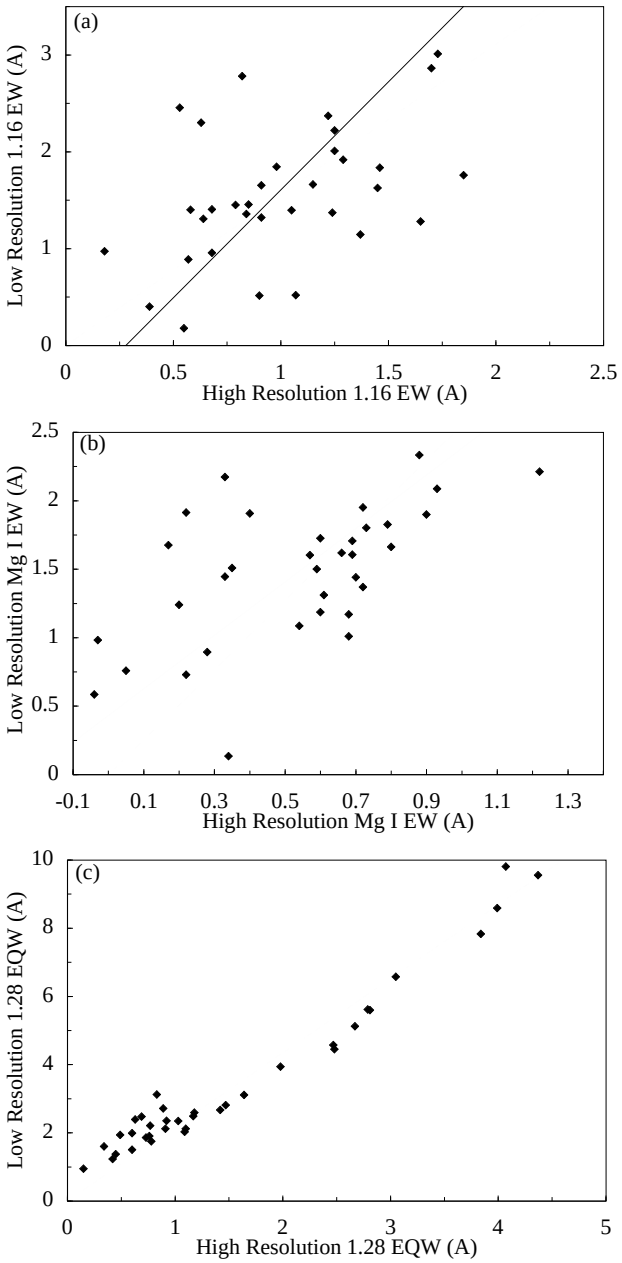

Fig. 4.— High resolution equivalent width (W2000) versus the low resolution equivalent width measured using our technique for the (a) 1.16 μm, (b) Mg I, and (c) 1.28 μm features. The solid lines are the fits with no constraints on the y-axis intercept given by equations 1.1 and 1.3 for (a) and (b), respectively. The dashed lines are the fits with a forced y-intercept of zero given by equations 1.2, 1.4, and 1.5 for (a), (b), and (c), repsectively.

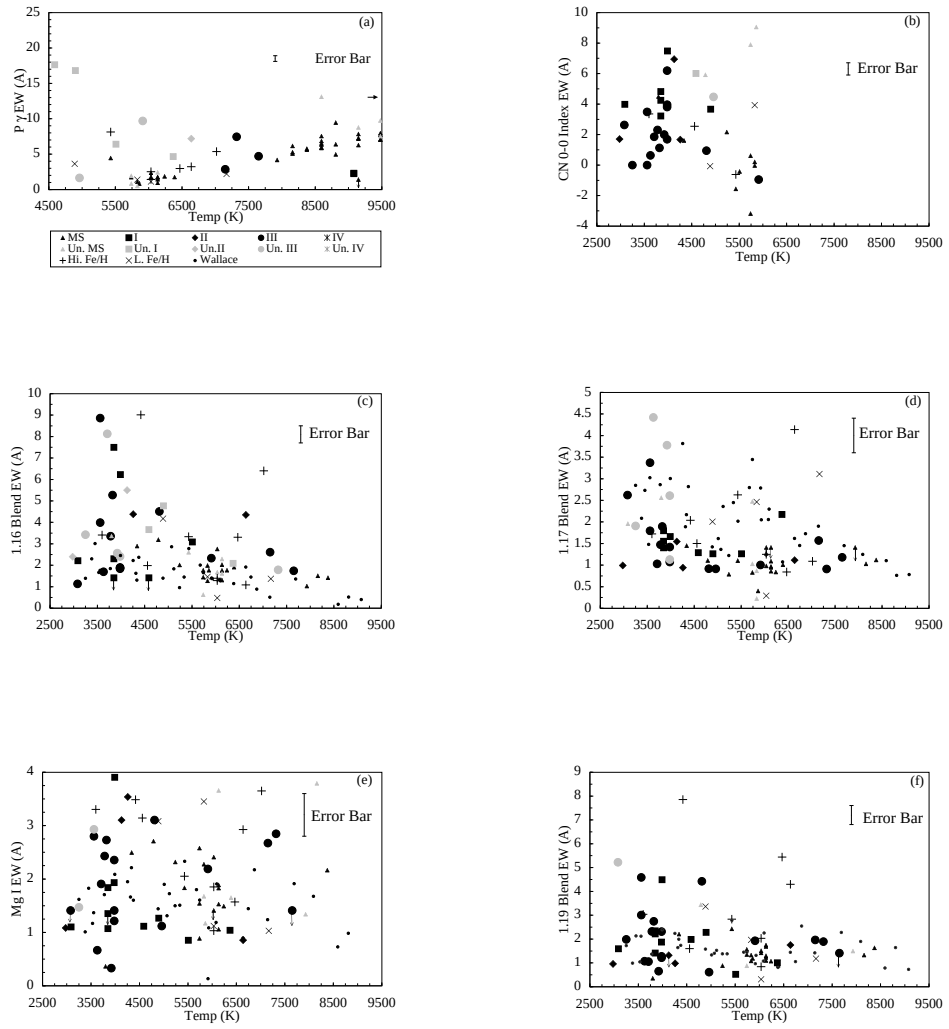

Fig. 5.— Equivalent width versus temperature in degrees Kelvin for the (a) Paschen γ, (b) CN index, (c) 1.16 μm, (d) 1.17 μm, (e) Mg I, (f) 1.19 μm, (g) 1.20 μm, (h) Si I, (i) 1.21 μm, (j) 1.28 μm, (k) 1.31 μm, and (l) 1.33 μm features. Solid black squares, diamonds, large circles, asterisks, and triangles represent luminosity class V, I, II, III, and IV respectively. The same symbols in gray represent stars in the respective luminosity class with uncertain equivalent measurements (σ(EW) > 0.4 Å). Crosses are stars with known high metallicity and "x" represents stars known to have low metallicity. All small circles are our measurements of spectra published by W2000 (see § 5). An error bar is shown in the right corner to represent the equivalent width error that would be placed on each of the data points from our sample with a confident measurement (black symbols). Horizontal arrows in (a) and (j) indicate more data exists at greater temperatures, but have not been included in the plot.

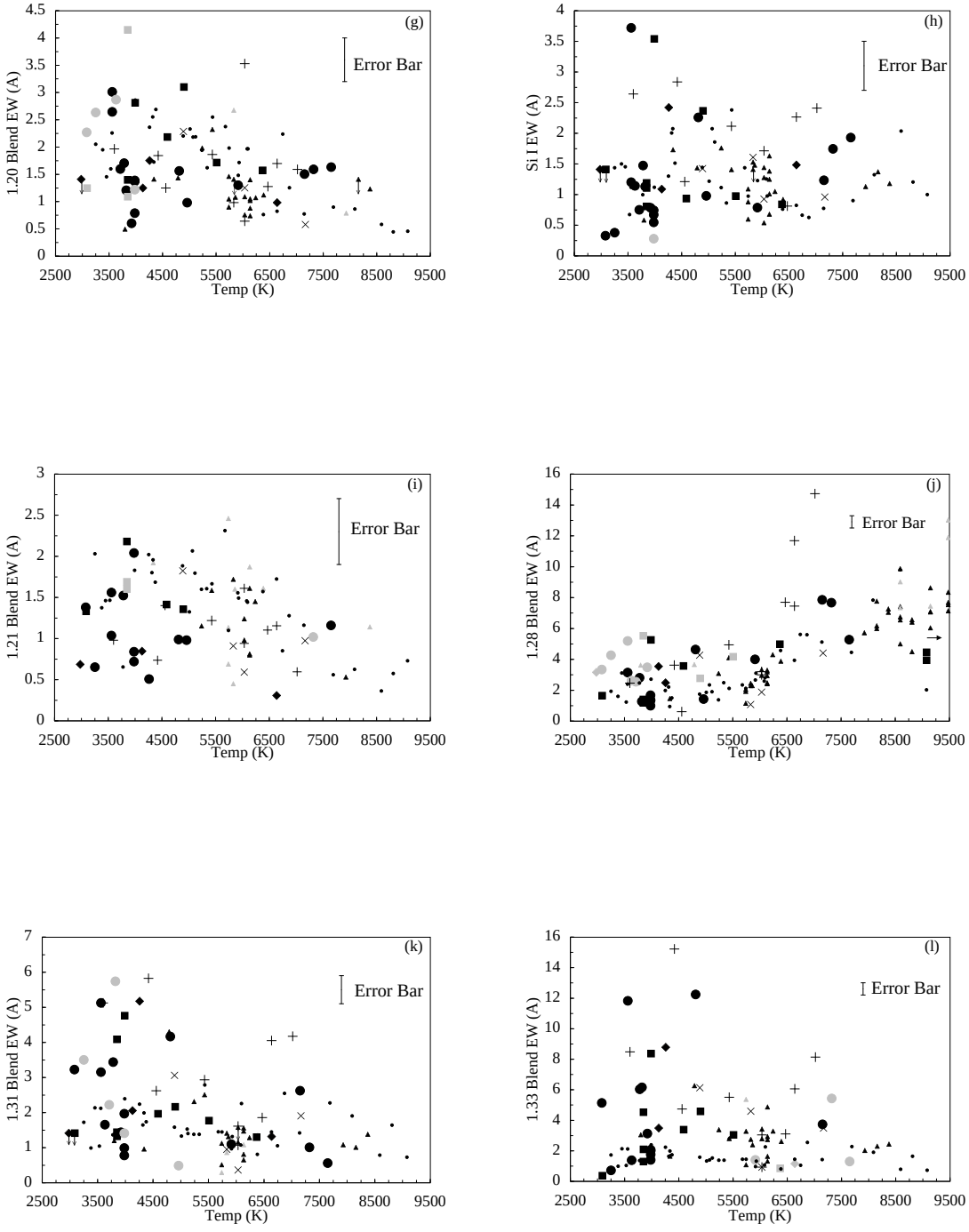

Fig. 5.— - *Continued*

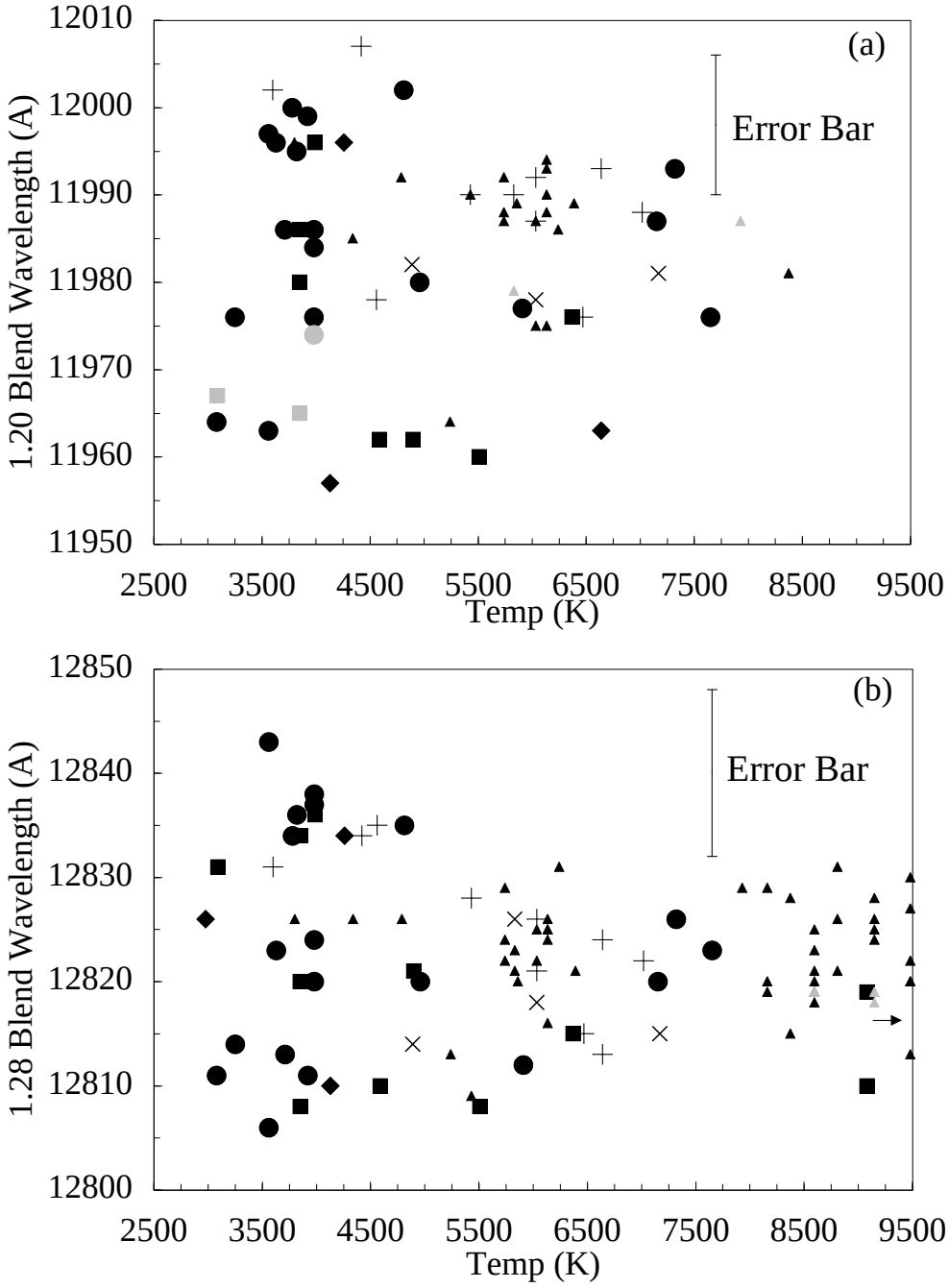

Fig. 6.— Central wavelength versus temperature in degrees Kelvin for the (a) 1.20 μm and (b) 1.28 μm features. See legend in Figure 5. An error bar is shown in the right corner to represent the central wavelength error that would be placed on each of the data points from our sample with a confident measurement (black symbols).

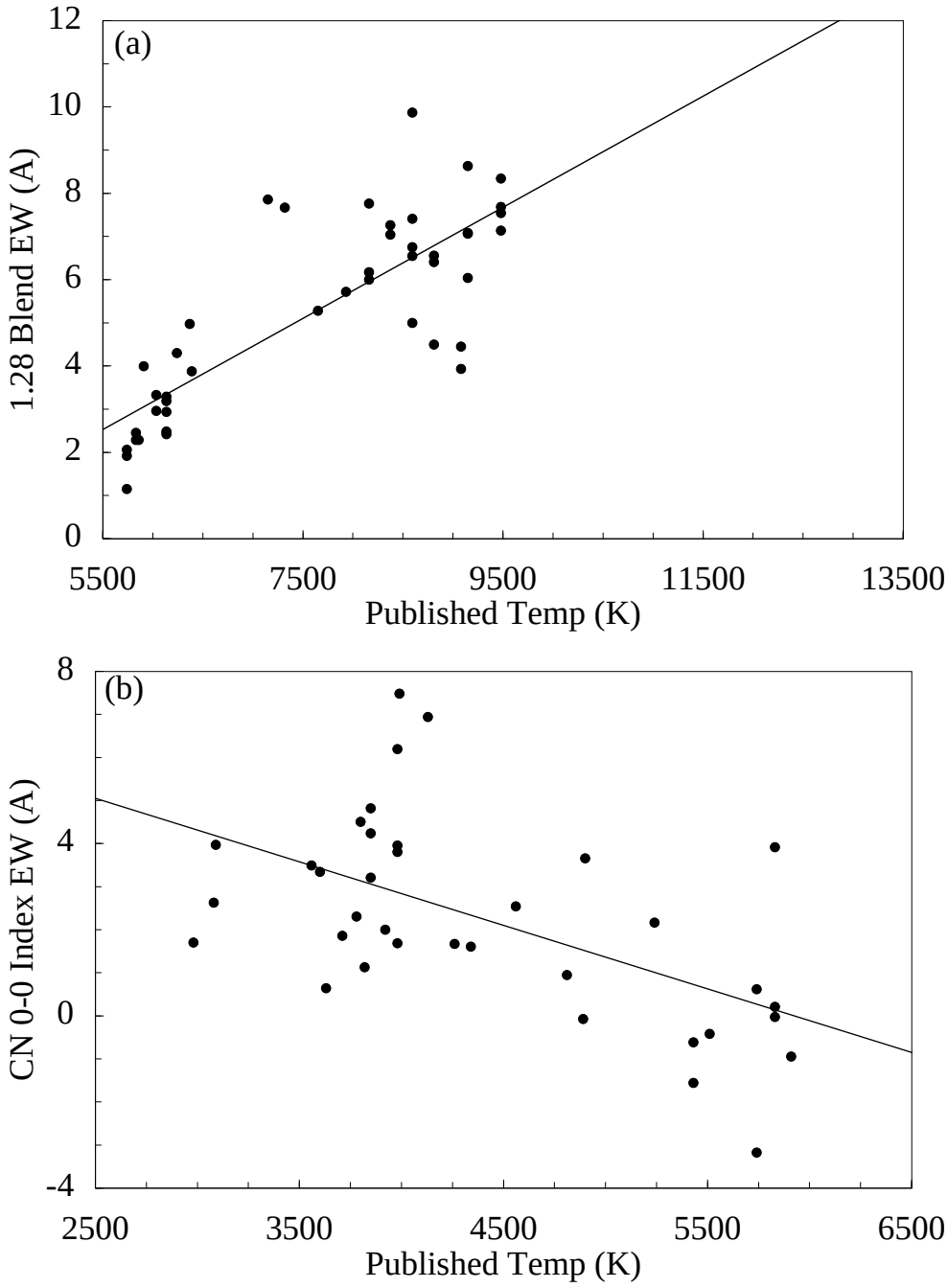

Fig. 7.— Equivalent width versus the published temperature for all stars except those with uncertain equivalent width measurements (σ(EW) > 0.4 Å) or high/low metallicity (see § 5.3). (a) 1.28 μm blend for temperatures greater than 5500 K and less than 9500 K. The solid line is the fit given by Equation 2. (b) CN index for temperatures less than 6000 K. The solid line is the fit given by Equation 3.

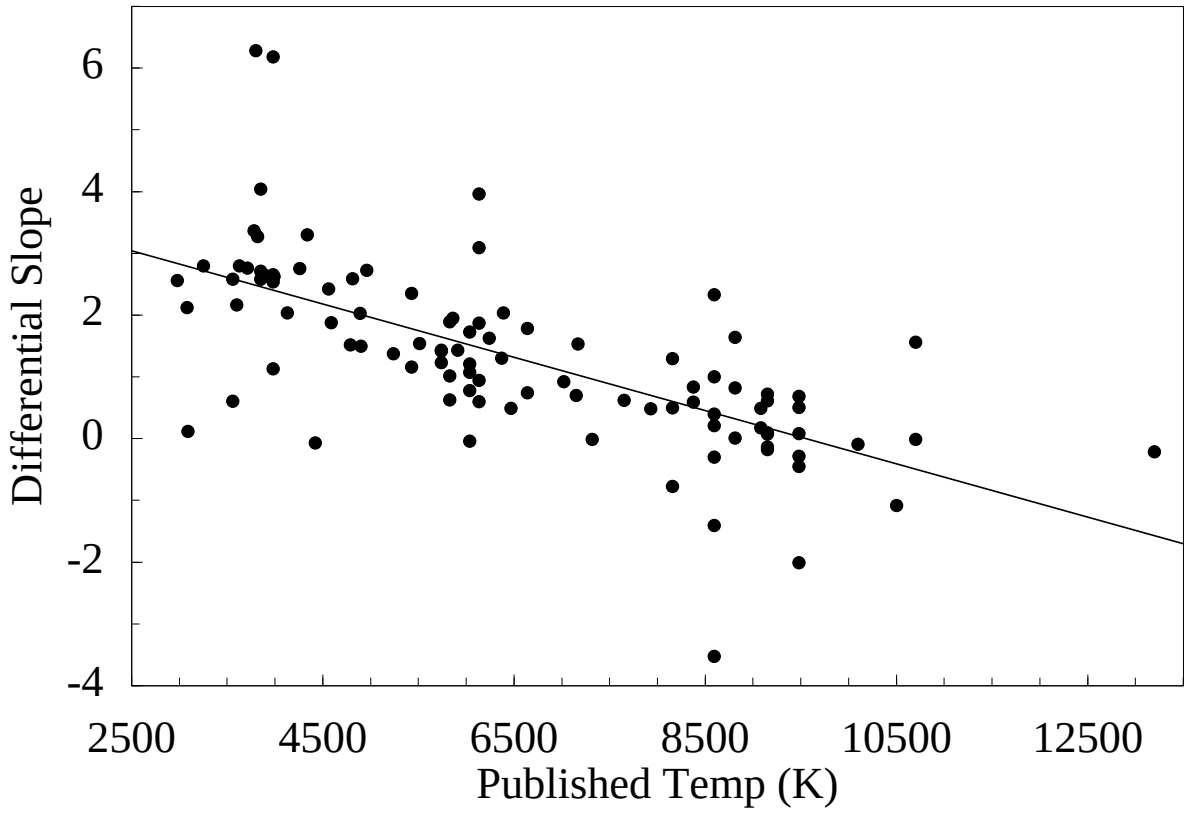

Fig. 8.— Differential slope of the stellar spectra versus the published temperature for temperatures less than 13500 K. The solid line is the fit given by equation 4.

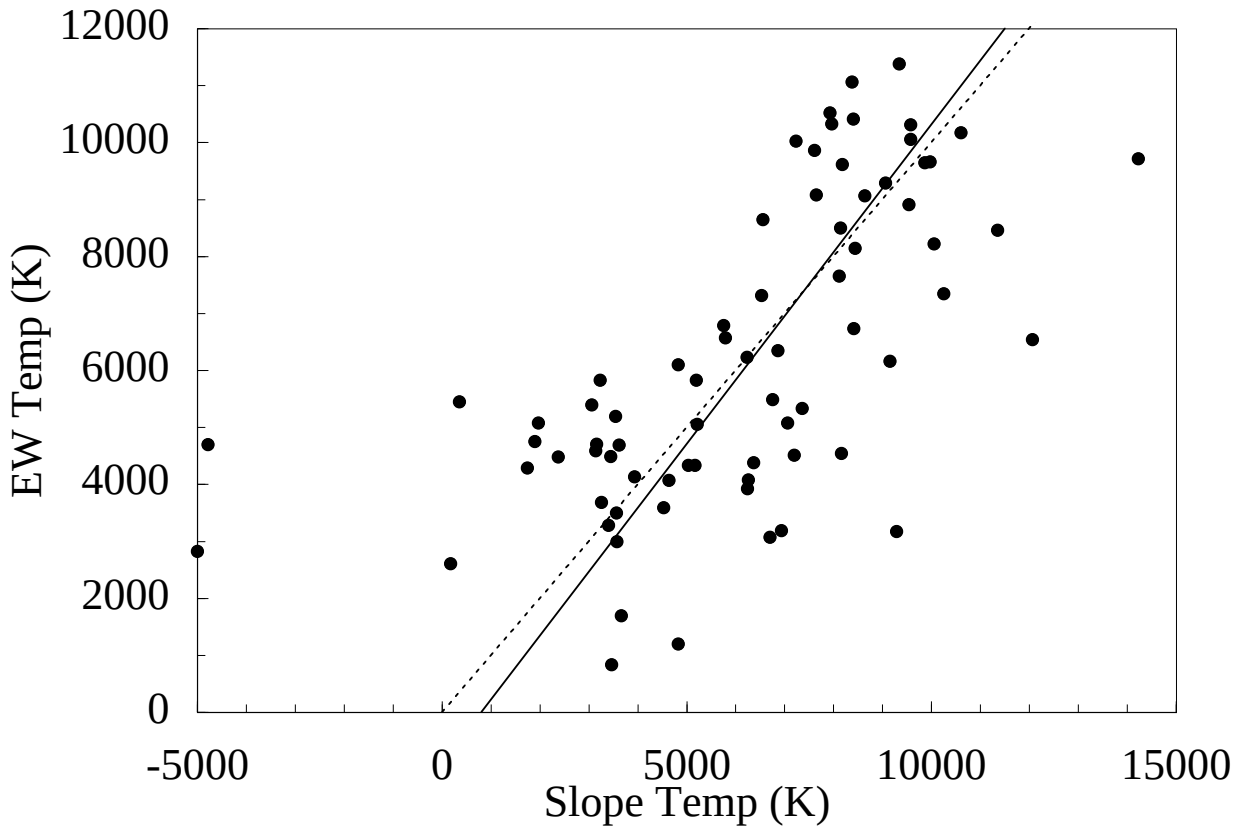

Fig. 9.— Temperature determined from the equivalent width versus the temperature determined from the slope of the spectrum. The solid line is the fit to the data and the dashed line is a one to one line.

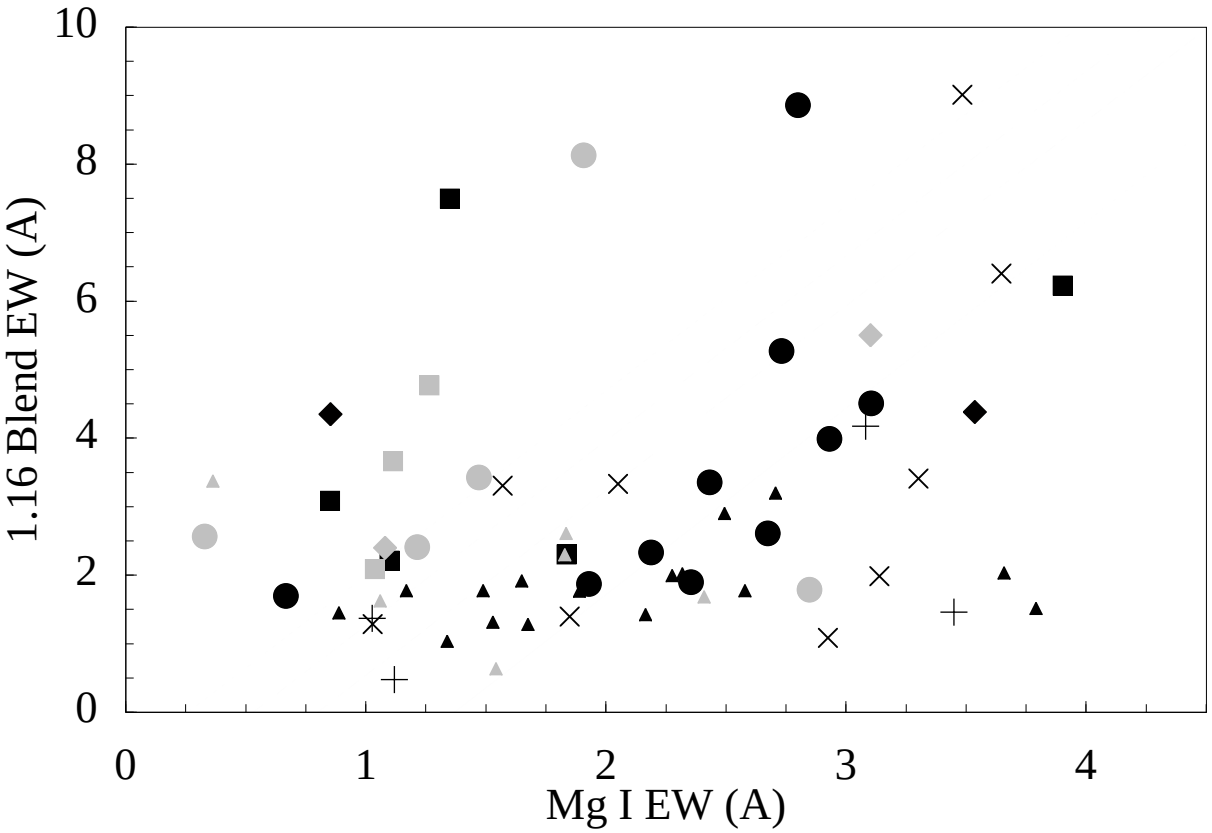

Fig. 10.— Equivalent width of Mg I versus the equivalent width of 1.16 μm. The solid line is a fit to the main sequence, the large dashed line is a fit to III, the medium dashed line is a fit to II, and the smallest dashed line is a fit to I luminosity class stars. The fit is that given in equation 6. See legend in Figure 5.

This figure "f3a.gif" is available in "gif" format from:

http://arxiv.org/ps/astro-ph/0204220v1

This figure "f3b.gif" is available in "gif" format from:

http://arxiv.org/ps/astro-ph/0204220v1

This figure "f3c.gif" is available in "gif" format from:

http://arxiv.org/ps/astro-ph/0204220v1

This figure "f3d.gif" is available in "gif" format from:

http://arxiv.org/ps/astro-ph/0204220v1

This figure "f3e.gif" is available in "gif" format from:

http://arxiv.org/ps/astro-ph/0204220v1